Toward Lateral Length Standards at the Nanoscale Based on Diblock Copolymers

Towards Lateral Length Standards at the Nanoscale Based on DiBlock Copolymers

Giulia Aprile,[a,c,*] Federico Ferrarese Lupi,[a,b] Matteo Fretto,[a] Emanuele Enrico,[a] Natascia De Leo,[a] Luca Boarino,[a] Flavio Giovanni Volpe,[b] Gabriele Seguini,[b] Katia Sparnacci,[c] Valentina Gianotti,[c] Michele Laus,[c] Jørgen Garnæs,[d] Michele Perego [b,*]

[a] *Nanofacility Piemonte, Istituto Nazionale di Ricerca Metrologica, Strada delle Cacce 91, Torino 10135, Italy*

[b] *Laboratorio MDM, IMM-CNR, Via C. Olivetti 2, Agrate Brianza (MB) 20846, Italy*

[c] *Dipartimento di Scienze e Innovazione Tecnologica (DIST), Viale T. Michel 11, Università del Piemonte Orientale "A. Avogadro", INSTM, Alessandria 15121, Italy*

[d] *Danish Institute of Fundamental Metrology (DFM), Matematiktorvet 307, 1. Sal 2800 Kgs. Lyngby Denmark*

* E-mail: g.aprile@inrim.it, michele .perego@mdm.imm.cnr.it

Keywords: Block copolymer, PS-*b*-PMMA, directed self-assembly, graphoepitaxy, trench, thin film, thermal annealing, metrology

Abstract

The self-assembly (SA) of DiBlock Copolymers (DBCs) based on the phase separation into different morphologies of small size and high-density features is widely investigated as patterning and nanofabrication technique. The integration of the conventional top-down approaches with the bottom-up SA of DBCs discloses the possibility to address the gap in nano-structured lateral length standards for nano-metrology, consequently supporting the miniaturization processes in device fabrication. In this frame, we studied the pattern characteristic dimensions (*i.e.* center-to-center distance L_0 and diameter D) of a cylinder forming PS-*b*-PMMA (54 kg•mol^{-1}, styrene fraction 70%) DBC when confined within periodic SiO_2 trenches of different width (W, ranging between 75 and 600 nm) and fixed

length (l, 5.7 μm). The characteristic dimensions of the PMMA cylinder structure in the confined configurations were compared with those obtained on the flat surface (L_0 = 27.8 ± 0.5 nm, D = 13.0 ± 1.0 nm). The analysis of D as function of W evolution indicates that the eccentricity of the PMMA cylinders decreases as a result of the deformation of the cylinder in the direction perpendicular to the trenches. The center-to-center distance in the direction parallel to the long side of the trenches (L_{0l}) is equal to L_0 measured on the flat surface, whereas the one along the short side (L_{0w}) is subjected to an appreciable variation (ΔL_{0w} = 5 nm) depending on W. The possibility of finely tuning L_{0w} maintaining constant L_{0l} paves the way to the realization of a DBC-based transfer standard for the lateral length calibration with periods in the critical range between 20 and 50 nm where no commercial transfer standards are available. A prototype transfer standards with cylindrical holes were used to calibrate the linear correction factor $c(\Delta x')_{xx}$, of an atomic force microscope for a scan length of $\Delta x' = 1\ \mu m$. The relative standard uncertainty of the correction factor was only 1.3 % and a second order nonlinear correction was found to be significant.

Introduction

With the aim to maintain the economy of scale dictated by the Moore's Law, microelectronics is pursuing a dramatic downscale of the minimum feature size achievable in FinFETs and memory devices.[1–8] This miniaturization process requires the concomitant development of reliable characterization techniques and suitable standards for the dimensional characterization of structures having minimum features size at the sub-10 nm level.

Industry and calibration laboratories need step height and lateral length standards at the nanometric level for resolution certification of a variety of measuring instruments, such as Atomic Force Microscopes (AFM), Scanning Probe Microscopes (SPM), Optical Phase Shift Microscopes, and Scanning Electron Microscopes (SEM). The currently available standards for step height and lateral length measurement have two substantial drawbacks for their reliable use in nanofabrication technology: they are too large and their uncertainty level is not acceptable for the increasing needs of metrology. For example, step height measurements of less than 3 nm are required [9,10] whereas the smallest step height standard available on the market has a step height of h = 6 nm with an expanded uncertainty $U(h)$ ranging from 0.5 to 1 nm. The situation for lateral length standards is similar. In this case, periodical patterns are commonly used and the pitch i.e. the distance between two subsequent elements of the repeated nanostructures is used as a length standard. The uncertainty of the mean pitch could be of the order of few tenths of nanometers, since, in the determination of an instrument's non-linearity, an extremely high accuracy is needed.[11–13] No periodic structures are currently available as lateral length standard with period below 50 nm but above typical lattice spacing in the range of 1 nm. Commercial standards in this range of length consist of a small chip containing a single isolated line 4 mm long. The width of the line is certified by TEM analysis and used as a reference standard. The smallest line width ranges from 110 to 25

nm.[14] Due to the inherent limitations of the nanofabrication process the defectiveness of the line is of the order of 5%. Alternatively preferential etching at single-crystal silicon is used to produce structures with a defined sidewall angle along the silicon (110) lattice plane.[15] However, in all of these structures, only individual geometrical properties (line width, sidewall angle) are well defined which is not sufficient, as these standards cannot be used to assess the important lateral calibration and linearity on a small scale of SEM, AFM and SPM images. In particular AFM is used for accurate and traceable measurements of individual surface structures in the range below 100 nm. However, even if the AFM is equipped with distance sensors calibrated from images with side length of 10 μm this is not sufficient to assure accuracy and estimate uncertainty on a small scale. Imperfections in alignment of the distance sensors relative to the probing tip and mechanical hysteresis and creep in the metrology frame makes it necessary to assess specific the calibrating and associated uncertainty for images with side length smaller than 1 μm.

The implementation of traceable measurement capabilities in surface and material science or biophysics requires the introduction of new types of reference samples for length metrology at the nanoscale. In particular a new paradigm is necessary for the realisation of nanoscale lateral length standards, possibly employing invariants of nature, like lattice parameters and self-organized structures at the nanoscale. Advanced top-down nanopatterning techniques, such as Electron Beam Lithography (EBL) or Extreme-Ultra-Violet (EUV) lithography, can produce features having smaller pitch size. However the first technique is not directly exploitable to large area, and the second one has at the moment too high rejection rates when the size is less than 20 nm. One interesting alternative option to obtain well-ordered sub-20 nm features is represented by the use of self-assembled DiBlock Copolymers (DBCs). In these macromolecules the immiscibility of the two chemically distinct blocks results in a phase separation resulting in different morphologies characterized by a variety of periodic

structures (*e.g.* lamellae, cylinders, spheres) having typical feature sizes below 20 nm.[16–18] The characteristic dimensions of the self-assembled features can be easily tuned by properly varying the chain length of the DBC.[19–21] Moreover in the form of thin films, DBCs have attracted considerable interest as they are compatible with conventional fabrication protocols of semiconductor industries and, consequently, they could represent the operative tool for the development of dense, high aspect ratio patterns in the next generation of microelectronic, optoelectronic, and data storage devices.[22–26] In principle self-assembled DBC thin films are perfectly suited to fabricate a periodic polymeric template employable as a mask for subsequent additive or subtractive processing of the underlying substrate. In this way a periodic pattern can be generated on the whole surface of a silicon wafer and potentially used as a length standard.

Actually long range ordering has already been demonstrated in DBC thin films deposited on flat surfaces, with the formation of large periodic structures (grains) whose average size is of the order of hundreds of nanometers.[27–33] Nevertheless further improvements are mandatory in order to satisfy the stringent metrological requirements. For instance, the instrument calibration process requires measurement areas of the order of several micrometers to obtain an adequate statistic. A possible solution to improve the long-range order in the reference samples is provided by the so called directed self-assembly (DSA), i.e. the DBC self-assembly within prepatterned structures. Indeed, when the DBC is forced to arrange itself inside micrometer-long trenches, the long range ordering of DBCs can be substantially enhanced. In particular, the DBC order is maintained along the entire trench length. In addition, the DSA approach guarantees the formation of a periodic template with controlled characteristic dimensions.[34,35]

On a flat and properly neutralized substrate, the periodicity L_0 of the DBC thin film uniquely depends on its chain length. Conversely, when the polymeric film is confined inside

topographically defined trenches, L_0 is modified due to the rearrangement of the polymeric template to fill the space that is available within the trenches. [34–38] Significant variations of L_0 are observed depending on the geometrical parameters of the confining structure, *i.e.* trench width W and length l. In the case of sphere PS-*b*-PFS forming DBC films, it was demonstrated that, if W perfectly commensurates with the spacing r between two adjacent rows of spheres, a number of rows $N = W/r$ will be formed and the value of L_0 in the polymeric template within the trenches is equivalent to the one measured in DBC films ordered on a flat surface.[36] On the contrary, when the polymeric film is confined inside non-commensurate trenches, L_0 is forced to vary by stretching or compressing the polymeric chains in order to homogeneously fill the trenches with N or $N+1$ rows of spheres. The choice between the stretched or the compressed configuration is driven by the free energy of the DBC chains. [36] Similar results have been reported for lamellae forming DBC [34,39] and for a ternary blends of cylinder-forming PS-*b*-PMMA, PS and PMMA homopolymers.[40] Moreover in the case of sphere forming thin films, it has been demonstrated that, if $l >> W$, the effect of confinement is anisotropic, and consequently different values are observed when measuring L_0 in the direction along the long (L_{0l}) or short (L_{0w}) side of the trench. [35,36] However to fabricate a length standard for instrument calibration, the periodic template of the DBC film has to be transferred to the underlying substrate by means of a Reactive Ion Etching (RIE) process. In this respect, cylinder forming DBC are preferred over sphere forming DBC due to the enhanced aspect ratio of the polymeric mask that can be achieved using this specific configuration, providing more flexibility in terms of pattern transfer to the underlying substrate.

In this work, we investigate the possibility of using DBCs films as a lithographic tool for the realization of length standards for instrument calibration. We study in details the organization of cylinder forming polystyrene-*b*-polymethylmethacrylate (PS-*b*-PMMA) DBC thin films

confined within topographically defined trenches. We focus on gratings of multiple trenches to ensure a perfect confinement of the DBC thin film within the trenches.[41] Collected data allow defining the geometrical parameters (*W, l*) and operational conditions that guarantee the formation of a polymeric template consisting of a unique grain of hexagonally packed PMMA cylinders perpendicularly oriented with respect to the substrate. In particular we investigate variations in the periodicity of the polymeric template as a function of the width of the trenches in order to minimize the error in the definition of the L_0 value.

Experimental Details

Periodic pattern definition

A 100 nm thick thermal SiO_2 over a Si (100) substrate was used as a support. A resist (940 K PMMA) diluted in anisole at 4% was spin coated (6000 rpm) over the SiO_2 surface. Thereafter, the resist was subjected to a thermal treatment at 165°C for 5 min. The definition of the periodic topographic structures was achieved by EBL operating at 30 KeV. After the exposure to the e-beam at different current doses [$\mu C/cm^2$] the resist was developed in methyl isobutyl ketone: isopropyl alcohol (MIBK: IPA) 1:3 for 60 s, in isopropyl alcohol for 20 s, and finally rinsed in deionized (DI) H_2O. In order to systematically study the behavior of the DBC in the confined configuration, we designed groups of trenches (gratings) having a constant length (*l*) of 5.7 μm and variable width (*W)* ranging from 75 to 600 nm. Each grating was composed of ten trenches spaced by 100 nm. This space between two subsequent trenches will be addressed as *mesa* (*M*). Figure1a depicts a scheme of a single grating.

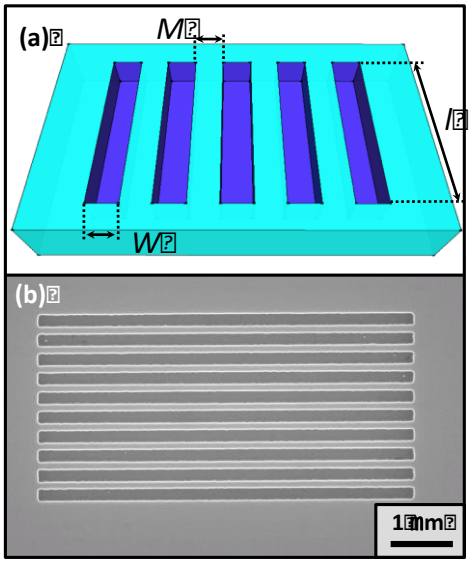

Figure 1: (a) Scheme of a trench array, where *W* is the trench width, *M* is the mesa structure among trenches and *l* is the trench length; (b) a representative SEM image of an array of SiO_2 trenches spaced 100 nm, a width of 250 nm and a length *l* of 5.7 μm.

After exposure and development of the resist, the EBL-defined patterns were transferred into the 100 nm thick silicon dioxide layer by RIE performed in a Plasmalab 80 Plus system at a pressure of 40 mTorr of a mixture of gases: CHF_3 (60 sccm) and Ar (25 sccm). The power of the RF generator was set at 120 W in order to etch the trench depth down to 90 nm. Finally, the samples were cleaned with a piranha solution (H_2SO_4:H_2O_2 3:1 vol. at 90 °C for 40 min) to eliminate any PMMA residuals and to increase the concentration of hydroxyl groups on the surface. The samples were then rinsed in DI H_2O, dried under a N_2 flow, cleaned with isopropanol in an ultrasonic bath, and finally dried again under N_2 flow. Figure1b shows a representative SEM image of a grating defined in the SiO_2 substrate, with width *W* = 250 nm spaced by mesas of *M* = 100 nm.

Surface Neutralization

In order to promote the vertical orientation of the PMMA cylinders in the DBC films, the SiO_2 surface was properly neutralized by means of a -OH terminated poly(styrene-*r*-methyl

methacrylate) random copolymer (RCP) (P(S-*r*-MMA)) with S fraction of 0.62, M_n = 1.7 kg•mol^{-1}, and PDI = 1.19. A solution of 18.0 mg RCP in 2.0 ml of toluene was firstly stirred in an ultrasonic bath, then filtered, and finally spun on the substrate for 30 s at 3000 rpm. This particular RCP system was chosen, in agreement with previous results reported in literature for the same DBC system,[42] in order to minimize the thickness of the grafting layer. To promote the grafting of the RCP on the SiO_2 surface, the thin film was thermally annealed at 310 °C for 60 s (heating rate 18 °C/s) in a commercial Rapid Thermal Processing (Jipelect JetFirst Series RTP) machine in a N_2 atmosphere. After the removal of the non-grafted chains with an ultrasonic bath in toluene, the thickness of the resulting RCP thin film on flat surfaces was measured to be 3.0 ± 0.1 nm by spectroscopic ellipsometry.

Block Copolymer Self-Assembling

An asymmetric PS-*b*-PMMA DBC 54 kg•mol^{-1}, PDI = 1.07, with a PS volume fraction of 0.71, was purchased by Polymer Source Inc. and was employed without further purification. This particular molecular weight corresponds to the cylinder-forming PS-*b*-PMMA DBC with the best trade-off between reduced characteristic dimensions and pattern uniformity over large area.[21] A periodic arrangement of hexagonally packed PMMA cylinders embedded in a PS matrix with L_0 = 27.8 ± 0.5 nm and D = 13.0 ± 1.0 was obtained.[21] It is worth to note that the possibility to promote phase separation in relatively low molecular weight PS-*b*-PMMA DBC was reported in the literature by different groups.[21,43–47] Nevertheless systematic investigations indicated that limited or negligible scaling of the characteristic lengths were achieved decreasing the molecular weight of the PS-b-PMMA DBC below the 54 kg•mol^{-1} limit. Moreover this limited reduction of the characteristic dimension is often associated with a lower lateral order. [18,21]

The DBC solution (18 mg in 2 ml of toluene) was treated in an ultrasonic bath and spun for 30 s at 3000 rpm on the grafted RCP layer, obtaining about 28 nm in thickness. The SA process was performed inside a RTP machine[48] at the annealing temperature, T_a 190 °C and 200 °C for 900 s. The SA dynamics at T_a = 190°C was investigated in a dedicated set of samples by systematically varying the annealing time t_a = 60, 120, 300, 600, and 900 s.

The fabrication of the nanoporous PS template was completed by a selective removal of the PMMA blocks. The degradation of the PMMA and contemporary the cross-linking of PS were promoted by an ultraviolet exposure (5 mW•cm^{-2}, λ = 253.7 nm, 15 min). A subsequent immersion in an acetic acid bath and a rinsing in DI H_2O selectively removed the PMMA. Finally, a 90 s of O_2 plasma treatment was performed to remove the RCP at the bottom of the pores.

Reactive Ion Etching process

The pattern transfer through the PS mask was carried out by means of a Reactive Ion Etching (RIE) process performed in CHF_3 (105 sccm) and Ar (44 sccm). The etching process was performed at a pressure of 1.15•10^{-2} mbar, with RF Power set at 300 W and bias voltage of 230 V. These parameters were chosen as a trade-off between physical and chemical etching, in order to minimize isotropic removal of material and heating of the PS mask, consequently avoiding modifications of the pristine hexagonal pattern.

Characterization techniques

The morphology of the polymeric films was characterized by SEM analysis using a Zeiss InLens system operating at an accelerating voltage of 15 kV. The thickness of the polymeric films was measured on flat samples by means of M-2000U spectroscopic ellipsometer (J. A. Wollam Co. Inc.) using a Xenon lamp and operating at an incident angle of 70°.

A dedicated software implemented by means of a Matlab routine was used for the analysis of the SEM images and the determination of the long range ordering of the DBC domains (the correlation length, ξ) on flat area as well as the measurement of the diameter (D) and the center-to-center distance (L_0) of the PMMA cylinders within the PS template on flat area and within the periodic trenches. In particular, the correlation length values were calculated following a method already reported in the literature.[49,50]

The L_0 values were measured following a software procedure analysis based on Delaunay Triangulation.[21] Initially, several high quality SEM images (pixel per nm ratio of about 0.27 and dimension 3.7 x 2.6 μm) were collected and subsequently processed by means of a Matlab routine that allows to measure the position of the PMMA cylinders in the PS matrix and to determine their relative distances. During this software analysis step, a binarization procedure was applied by means of a threshold operation which worked by scanning the image. After the binarization, the contiguous areas were detected specifying a interval of minimum and a maximum size. Thus the PMMA-cylinders were selected and the particles smaller or larger than this interval were ignored. Last cylinder identification procedure step was calculate the centroides of identified areas. Then Delaunay Triangulation was applied. In this specific procedure the SEM images were converted in set of points in a reference system (x,y) and each PMMA cylinder was inscribed in a circle. The coordinates (x_0, y_0) of each circle center were determined. Subsequently each point (x_0 y_0) was joined with its nearest neighbours following the Delaunay's law, i.e. maximizing the minimum interior angle of the triangles that were created linking each point. The result is a network of segments linked together. The length of each segment was measured and represents the center-to-center distance between first neighbor PMMA cylinders. The measured values of segment lengths were separated in two different groups as a function of their orientation with respect to the X axis that correspond to the long axis of the trenches. In this way, we obtained the values of L_{0l}

(segments parallel respect to the trench direction) and L_{0w} (segments perpendicular respect to the trench direction). The outputs of this procedure are two histograms representing the distribution of values of the measured distances. Finally, each distribution was fitted by a Gaussian distribution to determine the average center-to-center distance values for each family of trenches. The procedure was repeated for different values of the trench width in order to determine the evolution of L_{0l} and L_{0w} as a function of the trench width.

In order to keep roughly constant the number of analyzed PMMA cylinders and to ensure the detection of the entire area of a trench, for each set of trenches we acquired and analyzed from 2 up to 5 SEM images at 30kX. In this way, for our 5.7 μm long trenches, the average L_0 value determined from software analysis of the SEM images is the result of a distribution of L_0 values formed by $1.0 \times 10^4 - 2.0 \times 10^4$ data points. Moreover to estimate the error in the determination of L_0, we separately analyzed 4 images for each set of trenches with fixed width W. We determined the average L_{0l} value from each image. From these average values we calculated the standard deviation (σ) for a specific set of data and we obtained $\sigma < 0.1$nm. We repeated this operation for several sets of trenches, and we obtained the same value $\sigma <$ 0.1 nm for all the sets of trenches, irrespective of the trench width.

The example case of a calibration of an AFM was carried out on a state-of-the-art commercial microscope[51] optimized for wafer metrology and wafer inspection. In this microscope the scanning sample is mounted on a separate xy stage equipped with optical position sensors. For imaged with side length larger than 10 μm the microscope is calibrated using a two-dimension grating traceable to an international standard. On this two-dimensional grating the average period of nominal 1 μm was calibrated by laser diffraction. For imaging intermittent contact mode were used with sharp probes[52].

Results and Discussion

Optimization of the annealing parameters

The fabrication of a lateral length standard requires the accomplishment of a single DBC domain along the entire trench, without any defect in the block copolymer pattern or perturbation of the lateral ordering of the PMMA cylinders. To achieve this goal we initially investigated the long range ordering of the DBC domains on flat substrates and into the trenches as a function of the annealing temperature (T_a) and time (t_a).[53] In a previous paper, the long range ordering of the nanodomains on flat substrates was assessed by studying the evolution of the correlation length ξ as a function of the annealing temperature T_a. By increasing the T_a up to the degradation of the order in the DBC film, we demonstrated that the maximum processing temperature for this specific polymer on flat surfaces is T_a = 200 °C. [21]

In Figure 2a, a SEM plan view image of a DBC thin film annealed at T_a = 200 °C is reported. The corresponding colour map highlighting the grain boundaries was obtained by a software analysis and overlapped to the original SEM picture. The sample presents a very homogeneous morphology with PMMA cylinders perpendicularly oriented with respect to the substrate and relatively long range order (ξ = 200 ± 10 nm), in agreement with data reported in literature. [21] The situation significantly differs when the DBC is confined inside trenches topographically defined. Figure 2c shows a representative SEM plan view image of the DBC film inside a 210-nm-wide trench. The DBC film is partially detached from the walls of the trench and extended defective regions are present in the polymeric template. To overcome this issue and improve the regularity of the block copolymer template within the trenches we slightly reduced the annealing temperature to T_a = 190°C.

Figure 2b and Figure 2d report SEM plan view images of the DBC film annealed at T_a = 190 °C on a flat substrate and within a 210 nm wide trench, respectively. On the flat surface of the sample (Figure 1b) the extracted correlation length (ξ = 190 ± 10 nm) is equivalent, within the

experimental error, to that obtained at T_a = 200 °C. In the patterned region, no evidence of polymer degradation or film detaching is observed (Figure 1d). These observations led us to select T_a = 190 °C as process temperature for the subsequent experiments.

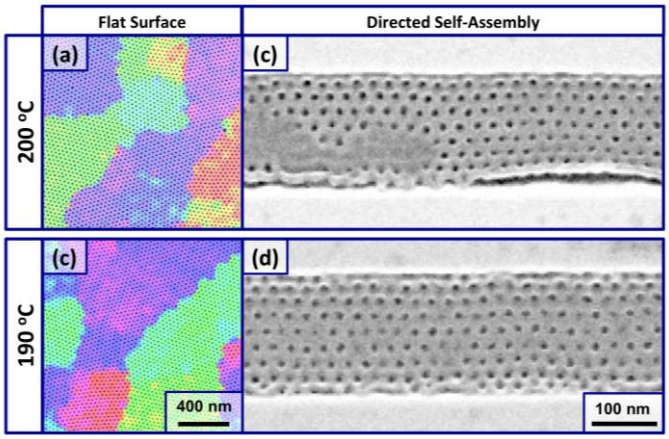

Figure 1. Colour maps and overlapped SEM images show the DBC thin film deposited on flat area and thermally annealed at (a) 200 °C and (b) 190 °C, respectively. (c)-(d) SEM images represent the morphology of the DBC film confined into trenches (W = 210 nm) and thermally annealed in a RTP machine at T_a = 200 °C and T_a = 190 °C, respectively.

It is worth to note that PMMA half-cylinders are clearly visible in proximity of trench sidewalls for both T_a. They are clear evidence of properly neutralized surface. Indeed, in agreement with the data reported in literature,[53] the P(S-r-MMA) RCP effectively neutralized the bottom and the walls of the trenches, promoting perpendicular orientation of the nanodomains in the trenches and half-cylinder formation on the sidewalls.

Once fixed the annealing temperature, the evolution of the lateral order on flat substrates and within topographically defined structures was investigated as a function of the annealing time. In particular, we focused on gratings of trenches with W ranging from 100 nm to 200 nm. The annealing time varied between t_a = 60 s and t_a = 900 s. Figure 3a reports some representative SEM plan view images obtained on samples annealed at three different t_a (120, 300 and 900 s). At each specific annealing time a different maximum value of W, that allows accommodating a single DBC grain structure, is observed. This condition is highlighted in

Figure 3a by the SEM images with black contour. Trenches with *W* immediately above this threshold value are characterized by the presence of multiple grains in the confined DBC films. Increasing the annealing time, the W value corresponding to the single grain limit also progressively shifts toward higher values. For instance in samples annealed at 190 °C for t_a = 120 s the single grain limit lies around *W* = 120 nm, while for t_a = 900 s such limit is extended to *W* = 200 nm.

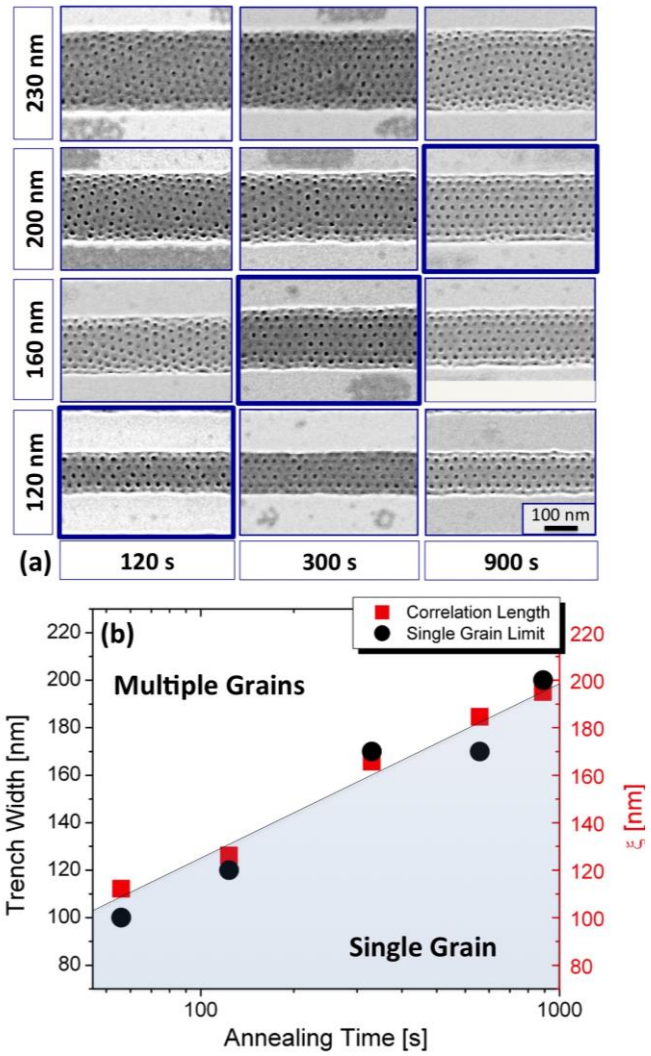

Figure 3. (a) SEM images representing trenches (230, 200, 160 and 120 nm in width) annealed at 190 °C for 120, 300 and 900 seconds. Increasing the annealing time, a single grain structure is observed for progressively wider trenches. (b) Correlation length measured on a flat area (red square) and single grain trench width (black circle) as a function of t_a.

The threshold values of trench width *W*, relative to a single grain in the confined DBC film, are reported as a function of t_a in Figure 3b. The corresponding values of the correlation length ξ measured on the flat surface are reported as well. Figure 3b clearly highlights a direct connection among the values of *W* corresponding to the single grain limit and the measured correlation lengths. There is a clear matching between the maximum width of the trenches that accommodate a single DBC domain and the ξ value measured on the flat surface after the same annealing time period.

In previous studies[48,53,54] we demonstrated that the achievement of a good lateral order in the DBC thin film, when confined within topographically defined trenches, was associated to the flowing of polymeric material from the mesa region into the trenches. Indeed this "back-wash effect" induces significant variation of the confined DBC film thickness. In particular we observed that the thickness of the confined DBC layer in a specific trench depends on the width of the *mesa* and on the position of the trench in the grating.[54] The *mesa* region and the area surrounding the gratings act as a reservoir of polymeric material that flows into the trenches during the thermal treatment, influencing the final DBC layer thickness. The maximum value of the DBC layer thickness is obtained when the surface surrounding the gratings is completely clean.

Figure 4 reports representative SEM images for a grating of 200 nm wide trenches and annealed at 190 °C for different t_a values ranging from 60 s to 900 s. In this case the width of the *mesa* is M = 100 nm. Increasing the annealing time, an evident reduction of the amount of polymer on the *mesa* surface is observed. Specifically, the analysis of the images indicates that the fraction of the *mesa* surface covered by the polymer corresponds to about 75, 38, 19, 6, and 0 % for t_a values of 60, 120, 300, 600, and 900 s, respectively. For the annealing time t_a = 900 s, all the polymeric material flowed from the mesa surface into the trenches, determining the achievement of a stable configuration with a constant thickness of the

confined DBC film. This result guarantees that no further perturbations of the lateral order in the confined block copolymer film are induced by the progressive introduction of additional polymeric material into the trenches. Moreover, thermally treating the samples at 190 °C for 900 s, independently of the progressive increase of DBC film thickness when moving from central to peripheral trenches, single grains are observed in all the trenches of the grating. This allows performing the analysis of the evolution of the lateral order in the confined DBC films independently from the position of the specific trench within the grating.

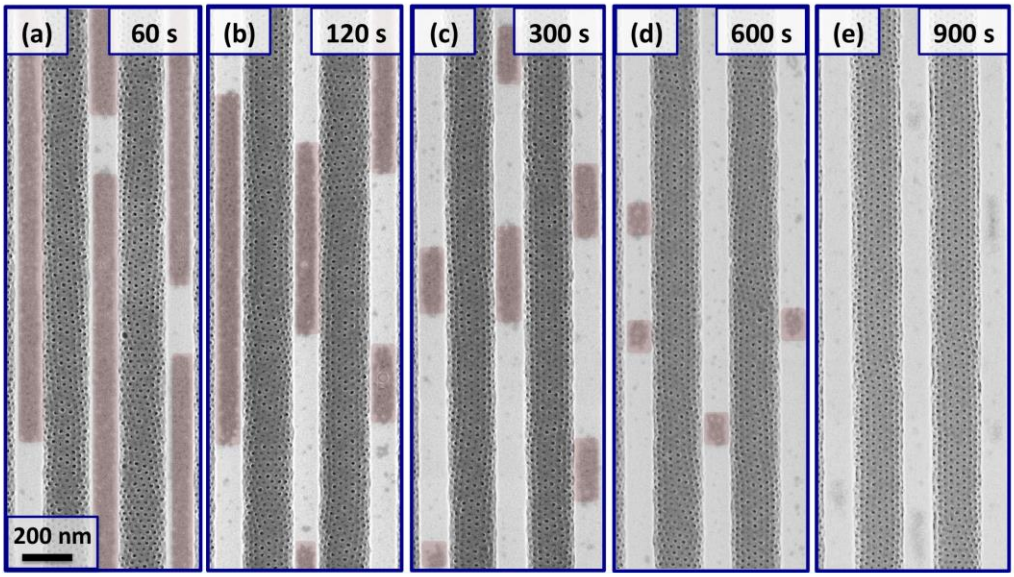

Figure 2. SEM images of 200 nm wide trenches as a function of the annealing time: (a) 60 s, (b) 120 s, (c) 300 s, (d) 600 s and (e) 900 s. The mesa (M = 100 nm) becomes cleaner increasing the annealing time.

PS-*b*-PMMA ordering in confined configuration

It is worth to remember that the formation of a single grain in the self-assembled polymeric film when confined within topographically defined trenches is strictly related to the commensurability between the trench width and the periodicity of the polymeric template.

Figure 5 shows a collection of SEM images of self-assembled DBCs (T_a = 190 °C, t_a = 900 s) confined within trenches of different width W, ranging from 90 nm to 200 nm. In these

images the values of *W* (190, 170, 140, 120, and 90 nm) well commensurate with DBC lattice parameters. The trenches accommodate a single DBC grain with no lattice defects and a constant number of cylinder rows along the entire trench length.

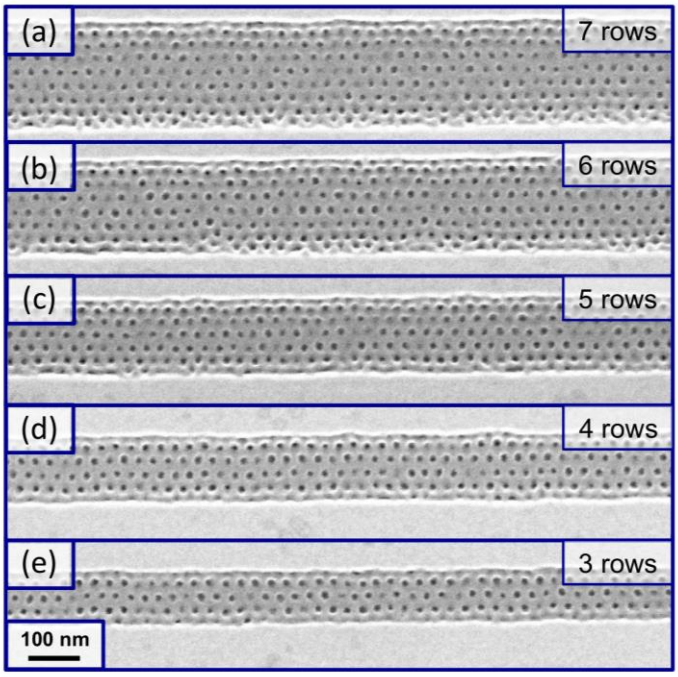

Figure 3. SEM images of trenches with different width, wherein it is possible to observe seven (a), six (b), five (c), four (d) and three (e) cylinder rows, respectively.

Conversely, if *W* is not well commensurate with the value of L_0, variations in the number of cylinder rows within the trenches are observed. The SEM plan view images in Figure 4 provide significant examples of trenches (*W* = 110, 130, 155, and 185 nm) wherein transitions from *N* to *N*+1 rows of cylinders are clearly observed. In particular, in 110 nm wide trenches we observed a turnover from three to four cylinder rows (Figure 4a), in 125 nm wide trenches a change from four to five (Figure 4b), in 155 nm wide trenches an alternation from five to six (Figure 4c), and finally in 190 nm wide trenches a variation from six to seven (Figure 4d). These variations in the number of rows within a trench take place when the DBC film does not exhibit a favourite arrangement (*N* or *N*+1 rows) with respect to the available space. For

$W \geq 200$ nm a clear variation in the number of rows is not observable because the effect of the topographical confinement is negligible and the DBC films self-assemble forming multiple grains, as previously described in Figure 3.

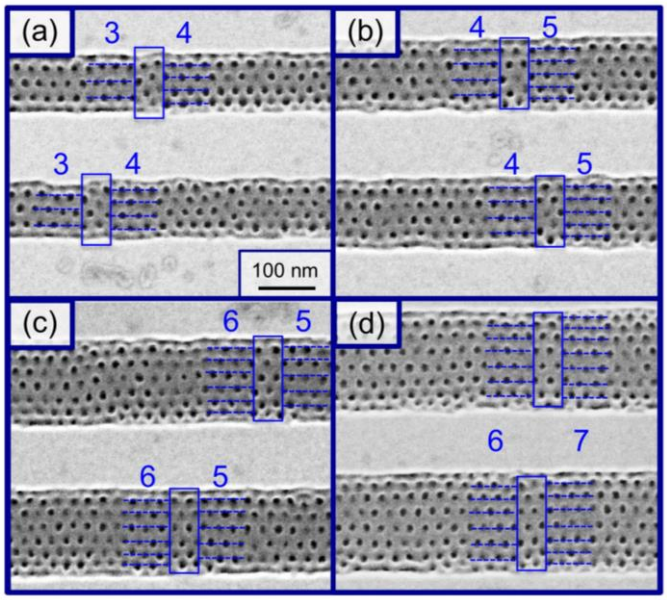

Figure 4. SEM images of trenches where the DBC changes the number of cylinder rows long the trench length. In the SEM images two example of changes, underline in blue dotted-line, are shown: three and four rows (a), four and five rows (b), five and six rows (c) six and seven rows (d). Inside blue rectangle is selected the film area where the transformation starts.

The bottom panel of Figure 7 (black points, right axis) reports the number of cylinder rows formed in the trenches as a function of W in a range from 75 to 250 nm. The experimental data were obtained considering the entire group of trenches forming the different gratings. As previously discussed for $W \geq 200$ nm we observe the formation of multiple grain within the trenches. Nevertheless extended regions of the polymeric film exhibit a good level of registration between the self-assembled template and the trenches. In the row-counting exercise, we considered these completely ordered areas only. Furthermore, in case the number of row is not constant within the trenches (Figure 6), for the corresponding W value, two black points are shown, linked with a vertical dark blue line.

The staircase trend of Figure 7 can be understood on the basis of a free energy model comparing the chain energies in confined and unconfined DBC films. As reported by Cheng *et al.*[36] the free energy of the polymeric film depends on the elastic strain energy and the blocks interfacial energy. The ratio between the free energy for a confined DBC chain (F_c) and the free energy for an unconfined DBC chain (F_0) is defined as:

$$\frac{F_c}{F_0} = \frac{1}{3}\left[\lambda^2 + \frac{2}{\lambda}\right]$$

where λ is the normalized period, i.e. the ratio between the *W** and *Nd*; *W** is the effective space available to accommodate the self-assembled DBC pattern and corresponds to *W* reduced by the thickness of the P(S-*r*-MMA) RCP and by the thickness of the PS-*b*-PMMA DBC half-cylinder formed on the walls of the trenches due to neutralized surface, called *s*. *N* is the number of cylinder rows and *d* corresponds to the distance between two adjacent rows of PMMA cylinders. In the film deposited on a flat substrate, i.e. in absence of stress or strain of the polymeric template, $d = (\sqrt{3}/2)\, L_0$. A schematic representation of all these parameters is reported in the top panel of Figure 7. In this way for each *N* value there is only a proper *W** matching the DBC lattice parameters. This *W** value corresponds to the condition $F_c/F_0 = 1.00$ indicating that the copolymer chains confined inside the trenches have the same free energy of the unconfined copolymer chains. If *W** is higher than a multiple of the bulk equilibrium period (*Nd*) the system is stretched. Otherwise if *W** is smaller than *Nd*, the system is compressed. The bottom panel of Figure 7 (coloured curves, left axis) shows the ratio F_c/F_0 value as a function of *W* for each specific *N* value. The ideal free energy DBC curves are reported as a function of *W* to facilitate the comparison with the superimposed experimental data. The calculated curves strictly match the experimental data.

For example, in case $N = 3$ the minimum value of the free energy curve corresponds to $W = 100$ nm. In the top panel of Figure 7 the SEM plan view picture of the PS-*b*-PMMA film confined within a 100 nm wide trench is reported. In the central part of the trench, three

cylinder rows are present with lattice parameters that perfectly commensurate with the measured effective width W^*. For W < 100 nm the F_c/F_0 ratio for the free energy curve corresponding to N = 3 progressively increases, crossing the free energy curve corresponding to N = 2 for about W = 85 nm. For this particular W value the DBC can indiscriminately arranges in two or three lines since the two configurations are energetically equivalent. Further decreasing the trench width W the system prefers to arrange itself in two rows rather than three since this configuration is energetically favoured. A similar reasoning applies for W > 100 nm, moving from N = 3 to N = 4.

The overall picture of the system indicates that, in general, if $W^* \approx Nd$, the polymeric template arranges within the trench to form N rows of cylinders. The transition in number of rows from N to N+1 occurs when $W^* \approx (N+0.5)d$. For this specific values of W^* the system can form polymeric templates with N or N+1 rows since the free energy of these two configurations is perfectly equivalent.

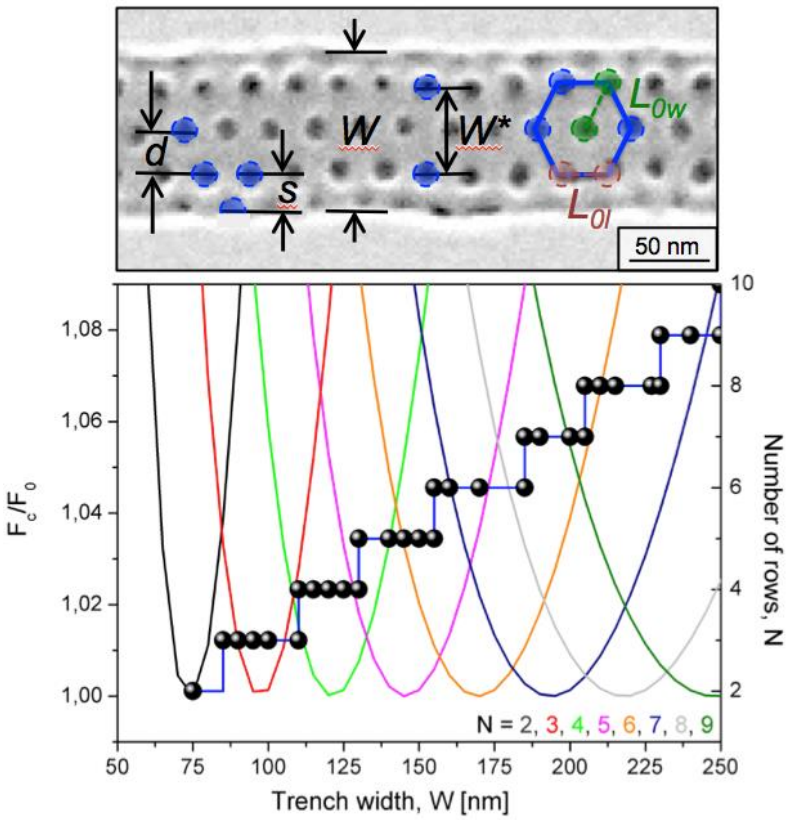

Figure 5. In the top panel, a schematic representation of the parameters involved in these studies: the distance *d* between two cylinder rows; the thickness *s* of the P(S-*r*-MMA) RCP and of the PS-*b*-PMMA DBC half-cylinder formed on the walls of the trenches due to neutralized surface; the trench width *W*; the effective space *W** available to accommodate the self-assembled DBC pattern; the center-to-center distance L_{0l} and L_{0w} between adjacent PMMA cylinders in the direction parallel and perpendicular to the long side of the trench. In the bottom panel, the calculated curves corresponding to the ratio between the free energy of the confined chains (F_c) respect and the free energy of the bulk chains (F_0). The values (left axis) are reported as a function of the *W* values. The measured number of rows (*N*) in the different trenches is reported as a function of *W* (right axis).

Center-to-center distance analysis

The regularity of the DBC pattern within the trenches was studied in details by investigating the evolution of L_0 as a function of *W*. In particular, we independently measured the two orthogonal components of L_0 along the long and the short sides of the trench, labelled L_{0l} and L_{0w}, respectively. Figure 8a reports the measured values of L_{0l} and L_{0w} as a function of *W*. The blue line corresponds to the value of L_0 measured in the block copolymer films deposited on the flat area of the sample. This value was found to be $L_{0F} = 27.8 \pm 0.5$ nm, that is in perfect agreement within the experimental error with the value found by GISAXS ($L_0^{GISAXS} = 28.3 \pm 0.3$ nm) analysis in our previous work for the same system on flat surface.[21]

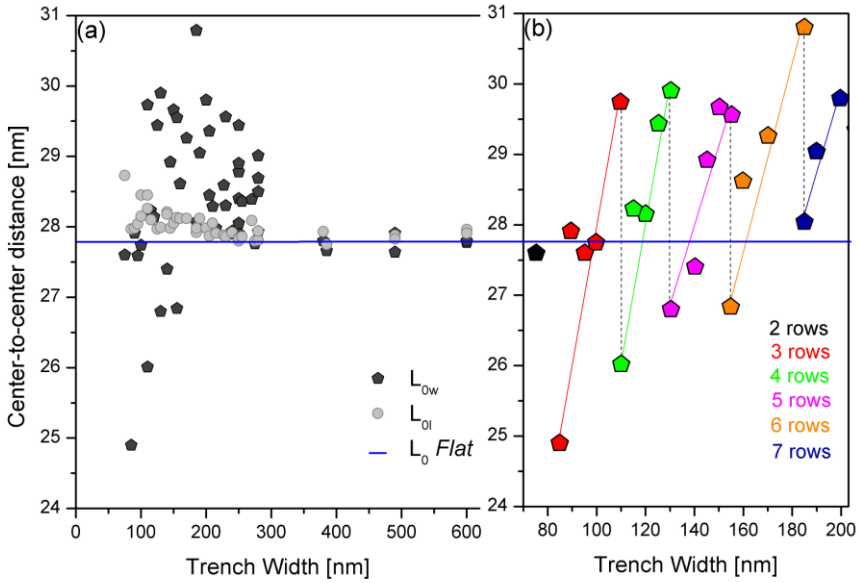

Figure 6. (a) Center-to-center distances (L_0) in the direction parallel (grey circles) and perpendicular (black pentagons) to the long side of the trenches are plotted as a function of W. (b) Variation of center-to-center distance L_{0w} as function of W is shown.

The L_{0l} values vary in a small interval between 27.8 and 28.7 nm (ΔL_{0l} = 0.9 nm) for W ranging from 75 nm to 300 nm. For W > 300 nm L_{0l} perfectly aligns to the L_{0F} value. The average L_{0l} is 28.0 ± 0.2 nm. Conversely, the L_{0w} values vary in a quite large interval ranging from 24.9 nm to 30.8 nm (ΔL_{0w} = 5.9 nm) for W values up to 300 nm. When $W \geq$ 300 nm, the L_{0l} and L_{0w} values are equivalent, within the experimental error, and match the L_{0F} value, consistently with the idea that the DBC films are not affected anymore by the confinement within the topographically defined structures.

Figure 6b focuses on L_{0w} variation for trenches with $W \leq$ 200 nm. Periodic oscillations of L_{0w} values as a function of W are clearly highlighted. This trend of L_{0w} is explained considering the effect of the confinement on the polymeric template. If the value of the trench width W satisfies the condition $W^* \approx Nd$, the polymeric template perfectly fits the trench and N rows of PMMA cylinders are formed without any distortion of the hexagonal lattice. This corresponds to the condition $L_{0w} = L_{0F}$. When the DBC film is confined in a trench with W

that does not commensurate with the periodicity of the polymeric template, the polymer is forced to adapt its lattice in order to fit the trench. According to this picture two different conditions are possible: if $Nd > W^*$ the polymeric template is compressed in the direction perpendicular to the trench long side. This compressive stress is reflected in a reduction of L_{0w} in comparison with L_{0F}. Conversely if $Nd < W^*$ the polymeric template is stretched to fill all the available space and consequently the L_{0w} value is higher than L_{0F}.

This evolution of L_{0w} is consistent with the free energy curves reported in Figure 7. If $Nd < W^* < (N+0.5)d$, the polymeric template arranges in N rows of cylinders since this is the configuration energetically favoured. Consequently a progressive stretching of the lattice, corresponding to an increase of L_{0w}, is necessary to fit the N rows into the trench when increasing W^* from Nd to $(N+0.5)d$. If $(N+0.5)d < W^* < (N+1)d$ the polymeric template arrange in $N+1$ rows of cylinders. This energetically preferred configuration implies a compression of the periodic lattice, corresponding to a decrease of L_{0w}, when W^* varies from $(N+1)d$ to $(N+0.5)d$. For $W^* = (N+0.5)d$ the DBC film can arrange in N or N+1 cylinder rows, because the two configurations are energetically equivalent. This specific condition was discussed in details in the case of Figure 6a. As a consequence two different L_{0w} values are observed within the same trench. In order to completely fill the trench, the polymeric template is subjected to a compressive or tensile stress in the case of the configuration with $N+1$ or N cylinder rows respectively. As shown in Figure 8b, these structural distortions of the polymeric lattice are clearly visible for $W \leq 200$ nm. Conversely, for $W > 200$ nm, DBC films exhibit multiple grains with various orientations in the same trench, since the system is not forced to align with the topographically defined structures.

In view of the realization of a final lateral length standard some further steps must be accomplished, such as the pattern transfer of the polymeric mask into a more stable matrix (such as SiO_2 or Si) and the evaluation of the uncertainty budget of the selected measurand (i.e. L_{0l}).

To check if the pattern-transfer process induces some changes on the final periodicity of the lateral length standard, we performed a RIE process though the confined PS mask. Subsequently we compared the center-to-center distance of the hexagonally packed cylinders calculated before the RIE process and after the pattern transfer into the SiO_2. The results of this study are summarized in Figure 9, in which two SEM images and the respective L_{0l} Gaussian distributions are reported.

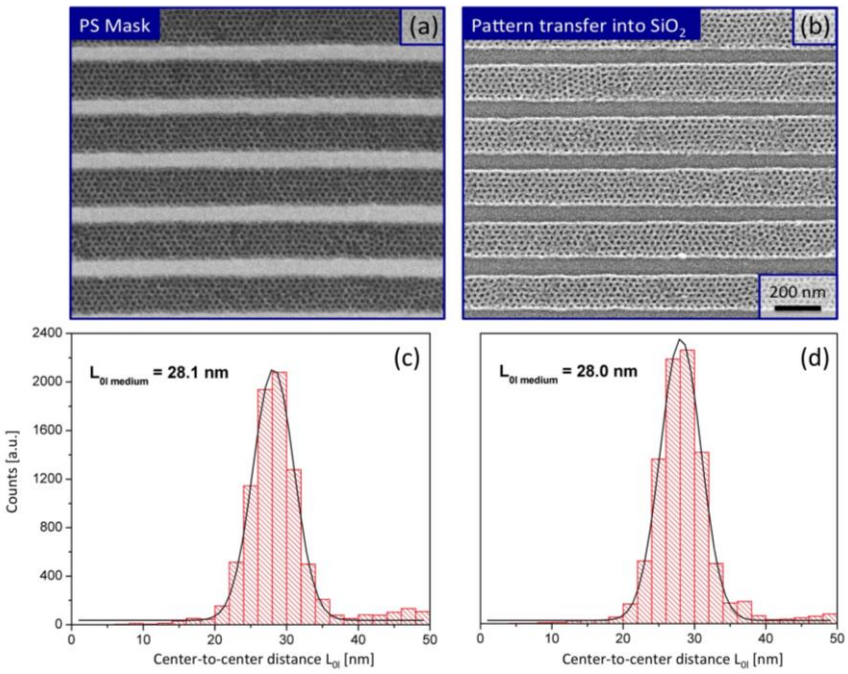

Figure 7. (a) Hexagonal BCP pattern confined inside the tranches before the RIE process (a) and resulting pattern transferred into SiO_2.

The L_{0l} value is 28.1 ± 0.5 when measured on PS mask and 28.0 ± 0.6 when measured on the SiO_2 transferred pattern. These two data perfectly match with the L_{0l} values previously measured, within the experimental error.

This check definitively reinforces the applicability of block copolymers as a lithographic mask and RIE as a technique able to accurately reproduce the characteristics of the polymer film on underlying substrate.

Calibration of an AFM

The next step toward the realization of a lateral length standard at nanometric level is the definition of a procedure for the calibration of an instrument, such as and AFM system. The general principles of calibration of an AFM based on transfer standards are described in e.g. reference [55] and [56]. Based on these principles a tailored set of calibration factors to correct the observed image along the x-direction is summarized below. Furthermore a calibration procedure of the x-axis is outlined, actual correction factors is calculated for the AFM system used and the associated calibration uncertainty is estimated based on a detailed discussion of an uncertainty budget.

Based on the principles reported in [55] and [56] the corrected position along the x-direction *x* can, as an approximation, be written as the first two terms in a Taylor expansion

$$x = c(\Delta x')_{xx'} x' + c(\Delta x')_{xx'^2} x'^2 + \ldots$$

where x' is the observed position along the x-direction and $c(\Delta x')_{xx'}$ and $c(\Delta x')_{xx'^2}$ are correction factors to be determined during calibration for a specific side length $\Delta x'$ of an image. In this case the linear correction factor $c(\Delta x')_{xx'}$ is approximated by

$$c(\Delta x')_{xx'} = \frac{L_0{}^{GISAXS}}{L_0{}^{Obs}}$$

where L_0^{Obs} is the average centre-to-centre distance observed in an image recorded by the AFM, while L_0^{GISAXS} is the reference value traceable to the SI unit for the centre-to-centre distance, determined in the present case by grazing-incidence small-angle X-ray scattering (GISAXS) experiments.

In order to calculate the uncertainty all significant influence parameters have to be included in a model function given as

$$c(\Delta x')_{xx'} = \frac{L_0^{GISAXS}}{L_0^{Obs} + \delta_{Sampl} + \delta_{Tip} + \delta_{Exp} + \delta_{ImagPro}}$$

where δ_{Sampl} is the deviation of the observed average centre-to-centre distance in the AFM image due to the limited number of cylinder holes in the image, while δ_{Tip} represents the deviation due to tip shape, deformation of the sample and uneven friction of the tip. Furthermore the contribution to the deviation due to different thermal expansion in the different part of the microscope and the possible deviation due to different gain value for the feedback loop is represented by δ_{Exp} while the deviation due to the image processing (including levelling and resolution of the AFM image) and the lack of accuracy of the algorithm used to identify the exact position of a cylinder hole is counted in $\delta_{ImagPro}$. It is worth to note that ideally the tip shape does not influence the observed centre-to-centre distance if the cylinder holes have identical surface shape.

In order to calibrate the AFM, the trenches in the prototype standard are aligned along the scanning direction to be calibrated e.g. the x-direction. An explicative example can be observed in Figures 10a and 10b, in which are reported AFM micrographs of the side length $\Delta x'$ to be calibrated (e.g. $\Delta x'$ = 1 μm).

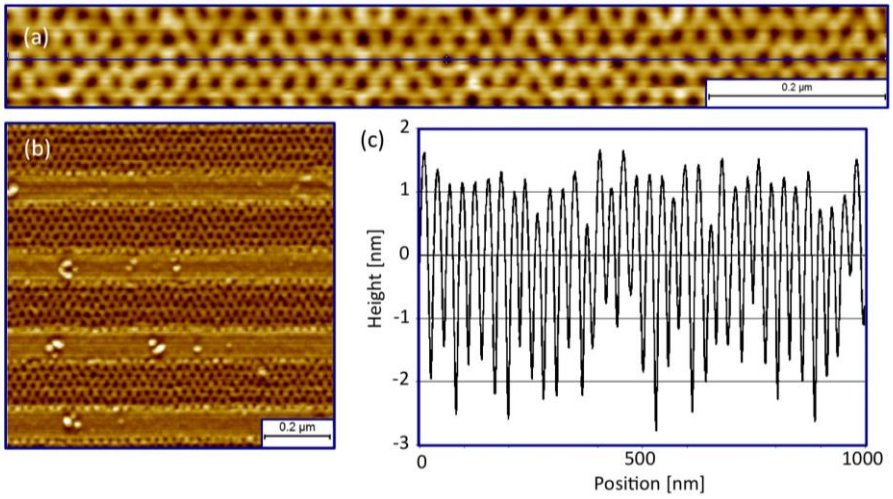

Figure 10. (a)-(b) AFM micrographs corresponding to the DBC patten confined inside the periodic trenches. (c) Height profile through the blue line marked in (a).

The position of each cylindrical hole and the average centre-to-centre distance of closest holes are calculated from the average profiles along rows of cylindrical holes along the x-direction similar to the profile of Figure 10c. The position of each hole is calculated as the position of the "centre of mass" of the area of the profile below an average line. The calculations are consistent with the positions found by commercial image processing software[57]. The measured values for the average centre-to-centre distance observed in an image with a side length of $\Delta x' = 1$ µm is given in Table 1, along with the reference value used and the standard uncertainty of the influence parameters. For the specific scan range investigated of $\Delta x' = 1$ µm and the microscope used the linear correction factor $c(\Delta x')_{xx'}$ is calculated to be 1.05 with a relative standard uncertainty of only 1.3 %.

Quantity (unit)	x_i	$u(x_i)$
Observerd average center-to-center distance L_0^{Obs}	27.70	0.01
Average center-to-cemter distance of the DBCs L_0^{GISAXS}	28.30	0.30
Deviation due to the limited number of sampled distances δ_{Samp}	0	0.20
Deviation due to tip shape and friction δ_{Tip}	0	0.07

Deviation due to drift and experimental control parameters δ_{Exp}	0	0.11
Deviation due to leveling and image processing $\delta_{ImagPro}$	0	0.05
Linear correction parameter $c(\Delta x')_{xx'}$	**1.02**	**0.014**

Table 1. Input parameters and associated uncertainty for the estimation of the linear correction factor $c(\Delta x')_{xx'}$ for a scan length of $\Delta x'$ = 1 μm.

Assuming that the period of the cylinders are constant it is also possible to assess the nonlinearity of the image recorded. Figure 11 shows the measured x-position error relative to a constant period of the cylinder holes as function of x-position. From the figure it is concluded that the nonlinear correction factor $c(\Delta x')_{xx'^2}$ is significant and equal to $2.3 \times 10^{-5} \frac{\text{nm}}{\text{nm}^2}$. If the nonlinearity is not corrected the deviation of the measured period relative to the average period is up to 0.4 % at the edge of the image (x = 0 and x = 100 nm).

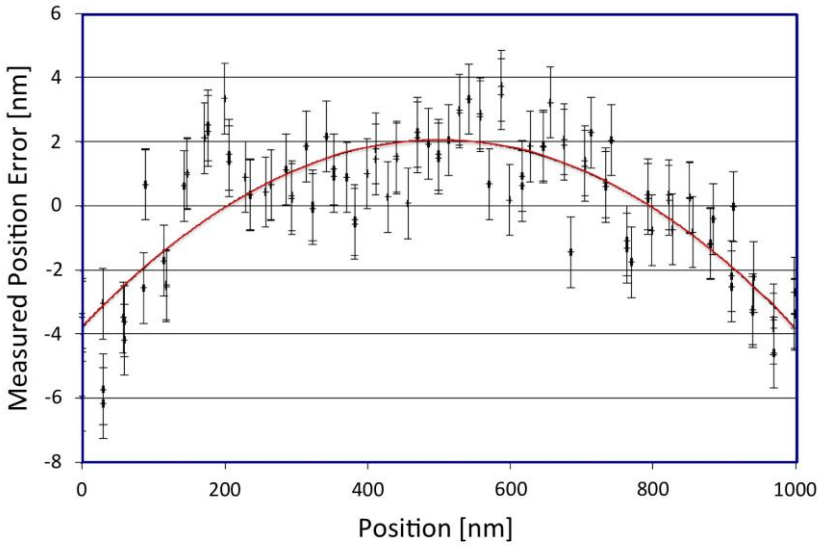

Figure 11. The measured position error relative to a constant period of the cylinder holes as function of position. The fitted polynomial has a significant second order coefficient of $2.3 \times 10^{-5} \frac{\text{nm}}{\text{nm}^2}$

Discussion

The collected results delineate an interesting scenario for the implementation of a metrological standard based on self-assembled DBC thin films. The natural periodicity of the hexagonally packed cylinder in the DBC template represents a simple system to calibrate lengths. The average periodicity L_0 of the nanoporous polymeric film is determined to be 27.8 ± 0.5 nm. When confined within topographically defined structures the template periodicity is preserved in the direction parallel to the trenches, irrespective of the characteristic dimension of the trenches themselves. Conversely significant variations of L_0 are observed in the direction perpendicular to the trenches due to stretching/compression of the polymeric film induced by the confinement within the topographically defined structures. Similar experimental evidence was reported by K.O. Stuen *et al.* [40] in the case of graphoepitaxial assembly of asymmetric ternary blends of block copolymers and homopolymers. By changing the composition of the blend it was possible to modify the periodicity of the periodic polymeric template and consequently to accommodate a different number of cylinder rows in topographically defined trenches with width 320 nm. Despite the compression/stretching occurring in the direction perpendicular to the trench walls, the periodicity in the direction parallel to the trench direction was not affected by the confining trench structure. Nevertheless no data were reported as a function of the trench width. Moreover it is worth to note that, considering our metrological target, the idea of controlling the periodicity of the self-assembled polymeric template by adding a homopolymer to the DBC does not represent a viable solution. The introduction of the homopolymer would make the process more complex with additional parameters (homopolymer characteristics and solution preparation) to be further adjusted in order to control the periodicity of the self-assembled polymeric template.

The variation of the periodicity in the direction perpendicular to the trench walls is associated to a stretching/compression of the PS block in the polymeric chains. This is accompanied by a

concurrent stretching/compression of the PMMA block that modifies the geometrical relationships among the PMMA cylinders. In order to evaluate this effect we define the eccentricity value of the cylinder structure as the ratio between the two axes of the ellipse containing the in-plane projection of the cylinder domain. On flat areas the eccentricity value is 0.9, indicating a circular cylinder placement. Conversely, when the DBC film is confined within the trenches, the eccentricity varies as a function of *W*. Indeed, when the DBC template well commensurates with the confining trench, the eccentricity value is close to 0.9. On the contrary, when the DBC film arranges in *N* or *N+1* rows within the same trench, the eccentricity decreases to 0.4 - 0.5 as a result of the deformation of the cylinder assembly in the direction perpendicular to the trenches.

The reproducibility of the experimental results has been verified by the fabrication of different test samples that exhibited the same L_{0l} values within the experimental error. This is consistent with the experimental data previously described. Actually data indicate that it is possible to relax the constrains on the definition of the trenches by top-down e-beam lithography, since the periodicity of the self assembled polymeric template is determined by the specific characteristics of the BCP and is essentially independent of the trench width. This prevents time consuming and complex procedures to precisely calibrate the lithographic process, since small variations in the trench width can be tolerated by the BCP without affecting the periodicity of the polymeric pattern. At the same time this tolerance guarantees the reproducibility of the periodic template, since the average L_{0l} value remains constant irrespective of small variations of the trench width among different batches. Actually we demonstrate that there is a reasonable large range of *W* values, close to commensurability with L_{0Flat}, that results in the formation of a single grain structure in the DBC template extending over the entire trench length. Within this set of values, L_{0l} is essentially constant and no variation in the number of rows ($N \rightarrow N + 1$) is observed in the DBC template, thus

significantly reducing the density of defects in the DBC lattice. Moreover, in agreement with data reported by Xiao et al.,[37] this analysis suggests that the roughness of the trench walls has a little impact on the intrinsic characteristics of the DBC pattern.

As a result of these combined effects, a strategy for the fabrication of a length standard for instrument calibration could be envisioned by decoupling the measurements in the two perpendicular directions (*x*, *y*) within the plane. Introducing two different families of gratings with trenches perpendicularly oriented one with respect to the other, it is possible to direct the block copolymer self-assembly process generating two groups of periodic polymeric templates. The length calibration in the *x* and *y* directions can be performed by measuring the periodicity L_{0l} of the self-assembled polymeric film along the long side of the trenches in the two families of gratings. This approach would allow increasing the accuracy of the calibration protocol, since the L_{0l} values is strictly related to the specific characteristics of the DBC and it is not influenced by small variations of the trench width. On the other side by increasing the length and the number of the trenches it would be possible to improve the precision of the measurements reducing the error in the determination of the L_{0l} parameter to a level compatible with the stringent requirements of a metrological standard.

In this regard it is worth to note that the fabrication of a length standard would require pattern transfer to the underlying substrate by means of anisotropic dry etching and this processes could affect the final template. Actually in this work we demonstrate that high fidelity pattern transfer of the polymeric mask to SiO_2 substrates capable to let invariant the L_{0l} is possible. This allows minimizing detrimental effects of the etching procedure on the final periodic structure that is used as length standard.

Conclusions

In this work we analyzed the possibility to fabricate a lateral length standard by means of direct self-assembly of confined DBC films within topographical structures. In particular, we used periodical trenches 5.7 μm in length and 90 nm in depth. The trench width was systematically varied from 75 to 600 nm. Asymmetric 54 kg•mol^{-1} PS-*b*-PMMA thin films were deposited on the samples. The self-assembly process was performed in a RTP system operating at T_a = 190 °C for t_a = 900 s. A single domain structure extending along the entire trench length was obtained only when *W* perfectly commensurates with the DBC center-to-center lattice parameter L_0. Interestingly we observed that this single domain structures were achieved only in the trench whose width values are smaller than the correlation length of the DBC film deposited on a flat substrate. We studied the evolution of the L_0 in the directions parallel (L_{0l}) and perpendicular (L_{0w}) with respect to the long side of the trench. The analysis of the data acquired as a function of *W* indicated that L_{0l} varies in a small interval between 27.8 and 28.7 nm. Conversely L_{0w} ranges from 24.9 nm to 30.8 nm. The possibility to carefully control these variations of L_{0w} and the restrained fluctuations of L_{0l} allow a strategy to use DBC as a tool for the fabrication of lateral length standards for probe microscopy instruments. A center-to-center distance analysis performed before and after the RIE process demonstrated that L_{0l} does not vary and the values remain within the experimental error.

A prototype transfer standards with cylindrical holes were used to calibrate the linear correction factor $c\,(\Delta x')_{xx'}$ for a scan length of $\Delta x' = 1\,\mu m$ with a relative standard uncertainty of only 1.3 %. A second order nonlinearity correction factor was found to be significant and estimated to influence with up to 0.4 % of the average period.

Acknowledgements

This research activity has been financially supported by the European Metrology Research Programme (EMRP), Project SiB61 CRYSTAL. The EMRP is jointly funded by the EMRP

participating countries within EURAMET and the European Union. Patent protection related to this work is pending.

References

(1) Collaert, N.; Alian, A.; Arimura, H.; Boccardi, G.; Eneman, G.; Franco, J.; Ivanov, T.; Lin, D.; Loo, R.; Merckling, C.; Mitard, J.; Pourghaderi, M. A.; Rooyackers, R.; Sioncke, S.; Sun, J. W.; Vandooren, A.; Veloso, A.; Verhulst, A.; Waldron, N.; Witters, L.; Zhou, D.; Barla, K.; Thean, A. V.-Y. Ultimate Nano-Electronics: New Materials and Device Concepts for Scaling Nano-Electronics beyond the Si Roadmap. *Microelectron. Eng.* **2015**, *132*, 218–225.

(2) Crupi, G.; Schreurs, D. M. M.-P.; Raskin, J.-P.; Caddemi, A. A Comprehensive Review on Microwave FinFET Modeling for Progressing beyond the State of Art. *Solid. State. Electron.* **2013**, *80*, 81–95.

(3) Sun, X. H.; Wang, S. D.; Wong, N. B.; Ma, D. D. D.; Lee, S. T.; Teo, B. K. FTIR Spectroscopic Studies of the Stabilities and Reactivities of Hydrogen-Terminated Surfaces of Silicon Nanowires. *Inorg. Chem.* **2003**, *42* (7), 2398–2404.

(4) Black, C. T.; Ruiz, R.; Breyta, G.; Cheng, J. Y.; Colburn, M. E.; Guarini, K. W.; Zhang, Y.; Heights, Y. Polymer Self Assembly in Semiconductor Microelectronics. *IBM J. Res. Dev.* **2007**, *51* (5), 605–633.

(5) Kim, H.; Park, S.; Hinsberg, W. D. Block Copolymer Based Nanostructures : Materials , Processes , and Applications to Electronics. **2010**, 146–177.

(6) Koo, K.; Ahn, H.; Kim, S.-W.; Ryu, D. Y.; Russell, T. P. Directed Self-Assembly of Block Copolymers in the Extreme: Guiding Microdomains from the Small to the Large. *Soft Matter* **2013**, *9* (38), 9059.

(7) Segalman, R. A.; McCulloch, B.; Kirmayer, S.; Urban, J. J. Block Copolymers for Organic Optoelectronics. *Macromolecules* **2009**, *42* (23), 9205–9216.

(8) Darling, S. B. Directing the Self-Assembly of Block Copolymers. *Prog. Polym. Sci.* **2007**, *32* (10), 1152–1204.

(9) Fu, J.; Tsai, V.; Koning, R.; Dixson, R.; Vorburger, T. Algorithms for Calculating Single-Atom Step Heights. *Nanotechnology* **1999**, *10* (4), 428–433.

(10) Suzuki, T.; Minoda, H.; Tanishiro, K.; Yagi, K. Single- and Triple-Height-Step Distributions on Si(111) Vicinal Surfaces Inclined toward [112] Studied by Reflection Electron Microscopy. *Surf. Sci.* **2002**, *496* (3), 179–186.

(11) Koenders, L.; Dziomba, T.; Thomsen-Schmidt, P.; Wilkening, G. Standards for the Calibration of Instruments for Dimensional Nanometrology. In *Nanoscale Calibration Standards and Methods: dimenional and related measurements in the micro- and nanometer range*; Wiley-VCH: Weinheim, FRG, 2005; pp 245–257.

(12) Dai, G.; Dziomba, T.; Pohlenz, F.; Danzebriink, H. U.; Koenders, L. Metrological AFMs and

Its Application for Versatile Nano-Dimensional Metrology Tasks. In *Sixth International Symposium on Precision Engineering Measurements and Instrumentation*; 2010; pp 7544–7546.

(13) Dai, G. L.; Koenders, L.; Pohlenz, F.; Dziomba, T.; Danzebriink, H. U. Accurate and Traceable Calibration of One-Dimensional Gratings. *Meas. Sci. Technol.* **2005**, *16* (6), 1241–1249.

(14) Guan, Y.; Tortonese, M. Metrology Standards for Semiconductor Manufacturing. In *7th International Conference on Solid-State and Integrated Circuits Technology*; 2004; pp 588–593.

(15) Novikov, Y. A.; Ozerin, Y. V; Rakov, A. V; Todua, P. A. Method for Linear Measurements in the Nanometre Range. *Meas. Sci. Technol.* **2007**, *18* (2), 367–374.

(16) Hobbs, R. G.; Farrell, R. A.; Bolger, C. T.; Kelly, R. A.; Morris, M. A.; Petkov, N.; Holmes, J. D. Selective Sidewall Wetting of Polymer Blocks in Hydrogen Silsesquioxane Directed Self-Assembly of PS-B-PDMS. *ACS Appl. Mater. Interfaces* **2012**, *4* (9), 4637–4642.

(17) Jung, Y. S.; Chang, J. B.; Verploegen, E.; Berggren, K. K.; Ross, C. A. A Path to Ultranarrow Patterns Using Self-Assembled Lithography. *Nano Lett.* **2010**, *10* (3), 1000–1005.

(18) Seguini, G.; Giammaria, T. J.; Ferrarese Lupi, F.; Sparnacci, K.; Antonioli, D.; Gianotti, V.; Vita, F.; Placentino, I. F.; Hilhorst, J.; Ferrero, C.; Francescangeli, O.; Laus, M.; Perego, M. Thermally Induced Self-Assembly of Cylindrical Nanodomains in Low Molecular Weight PS-B-PMMA Thin Films. *Nanotechnology* **2014**, *25* (4), 45301.

(19) Xu, T.; Kim, H. C.; DeRouchey, J.; Seney, C.; Levesque, C.; Martin, P.; Stafford, C. M.; Russell, T. P. The Influence of Molecular Weight on Nanoporous Polymer Films. *Polymer (Guildf).* **2001**, *42* (21), 9091–9095.

(20) Black, C. T.; Guarini, K. W.; Breyta, G.; Colburn, M. C.; Ruiz, R.; Sandstrom, R. L.; Sikorski, E. M.; Zhang, Y. Highly Porous Silicon Membrane Fabrication Using Polymer Self-Assembly. *J. Vac. Sci. Technol. B Microelectron. Nanom. Struct.* **2006**, *24* (6), 3188.

(21) Ferrarese Lupi, F.; Giammaria, T. J.; Seguini, G.; Vita, F.; Francescangeli, O.; Sparnacci, K.; Antonioli, D.; Gianotti, V.; Laus, M.; Perego, M. Fine Tuning of Lithographic Masks through Thin Films of PS-B -PMMA with Different Molar Mass by Rapid Thermal Processing. *ACS Appl. Mater. Interfaces* **2014**, *6* (10), 7180–7188.

(22) Sundrani, D.; Darling, S. B.; Sibener, S. J. Guiding Polymers to Perfection: Macroscopic Alignment of Nanoscale Domains. *Nano Lett.* **2004**, *4* (2), 273–276.

(23) Black, C. T.; Bezencenet, O. Nanometer-Scale Pattern Registration and Alignment by Directed Diblock Copolymer Self-Assembly. *IEEE Trans. Nanotechnol.* **2004**, *3* (3), 412–415.

(24) Hu, H.; Gopinadhan, M.; Osuji, C. O. Directed Self-Assembly of Block Copolymers: A Tutorial Review of Strategies for Enabling Nanotechnology with Soft Matter. *Soft Matter* **2014**, *10* (22), 3867–3889.

(25) Morris, M. A. Directed Self-Assembly of Block Copolymers for Nanocircuitry Fabrication. *Microelectron. Eng.* **2015**, *132*, 207–217.

(26) Frascaroli, J.; Brivio, S.; Ferrarese Lupi, F.; Seguini, G.; Boarino, L.; Perego, M.; Spiga, S. Resistive Switching in High-Density Nanodevices Fabricated by Block Copolymer Self-Assembly. *ACS Nano* **2015**, *9* (3), 2518–2529.

(27) Ferrarese Lupi, F.; Giammaria, T. J.; Volpe, F. G.; Lotto, F.; Seguini, G.; Pivac, B.; Laus, M.; Perego, M. High Aspect Ratio PS-B-PMMA Block Copolymer Masks for Lithographic Applications. *ACS Appl. Mater. Interfaces* **2014**, *6* (23), 21389–21396.

(28) Ceresoli, M.; Ferrarese Lupi, F.; Seguini, G.; Sparnacci, K.; Gianotti, V.; Antonioli, D.; Laus, M.; Boarino, L.; Perego, M. Evolution of Lateral Ordering in Symmetric Block Copolymer Thin Films upon Rapid Thermal Processing. *Nanotechnology* **2014**, *25* (27).

(29) Kim, S. H.; Misner, M. J.; Xu, T.; Kimura, M.; Russell, T. P. Highly Oriented and Ordered Arrays from Block Copolymers via Solvent Evaporation. *Adv. Mater.* **2004**, *16* (3), 226–231.

(30) Olson, D. A.; Chen, L.; Hillmyer, M. A. Templating Nanoporous Polymers with Ordered Block Copolymers †. **2008**, 869–890.

(31) Simão, C.; Khunsin, W.; Kehagias, N.; Salaun, M.; Zelsmann, M.; Morris, M. A.; Torres, C. M. S. Order Quantification of Hexagonal Periodic Arrays Fabricated by in Situ Solvent-Assisted Nanoimprint Lithography of Block Copolymers. *Nanotechnology* **2014**, *25*, 175703–175711.

(32) Yoo, H.; Park, S. The Fabrication of Highly Ordered Block Copolymer Micellar Arrays: Control of the Separation Distances of Silicon Oxide Dots. *Nanotechnology* **2010**, *21* (24), 245304.

(33) Bita, I.; Yang, J. K. W.; Jung, Y. S.; Ross, C. a; Thomas, E. L.; Berggren, K. K. Graphoepitaxy of Self-Assembled Block Copolymers on Two-Dimensional Periodic Patterned Templates. *Science* **2008**, *321* (5891), 939–943.

(34) Chen, W.; Luo, J.; Shi, P.; Li, C.; He, X.; Hong, P.; Li, J.; Zhao, C. Self-Assembling Morphologies of Symmetrical PS-B-PMMA in Different Sized Confining Grooves. *RSC Adv.* **2014**, *4* (92), 50393–50400.

(35) Cheng, J. Y.; Ross, C. A.; Thomas, E. L.; Smith, H. I.; Vancso, G. J. Templated Self-Assembly of Block Copolymers: Effect of Substrate Topography. *Adv. Mater.* **2003**, *15* (19), 1599–1602.

(36) Cheng, J. Y.; Mayes, A. M.; Ross, C. A. Nanostructure Engineering by Templated Self-Assembly of Block Copolymers. *Nat. Mater.* **2004**, *3* (11), 823–828.

(37) Xiao, S.; Yang, X.; Edwards, E. W.; La, Y.-H.; Nealey, P. F. Graphoepitaxy of Cylinder-Forming Block Copolymers for Use as Templates to Pattern Magnetic Metal Dot Arrays. *Nanotechnology* **2005**, *16* (7), S324-9.

(38) Hosaka, S.; Akahane, T.; Huda, M.; Zhang, H.; Yin, Y. Controlling of 6 Nm Sized and 10 Nm Pitched Dot Arrays Ordered along Narrow Guide Lines Using PS-PDMS Self-Assembly. *ACS Appl. Mater. Interfaces* **2014**, *6*, 6208–6211.

(39) Walton, D. G.; Kellogg, G. J.; Mayes, A. M. A Free Energy Model for Confined Diblock Copolymers. *Macromolecules* **1994**, *27* (21), 6225–6228.

(40) Stuen, K. O.; Detcheverry, F. a; Craig, G. S. W.; Thomas, C. S.; Farrell, R. a; Morris, M. a; de

Pablo, J. J.; Nealey, P. F. Graphoepitaxial Assembly of Asymmetric Ternary Blends of Block Copolymers and Homopolymers. *Nanotechnology* **2010**, *21* (49), 495301.

(41) Perego, M.; Andreozzi, A.; Vellei, A.; Ferrarese Lupi, F.; Seguini, G. Collective Behavior of Block Copolymer Thin Films within Periodic Topographical Structures. *Nanotechnology* **2013**, *24* (24).

(42) Sparnacci, K.; Antonioli, D.; Gianotti, V.; Laus, M.; Ferrarese Lupi, F.; Giammaria, T. J.; Seguini, G.; Perego, M. Ultrathin Random Copolymer-Grafted Layers for Block Copolymer Self-Assembly. *ACS Appl. Mater. Interfaces* **2015**, *7* (20), 10944–10951.

(43) Chevalier, X.; Nicolet, C.; Tiron, R.; Gharbi, A.; Argoud, M.; Prandelles, J.; Dealande, M.; Cunge, G.; Fleury, G.; Hadziioannou, G.; Navarro, C. Scaling-down Lithographic Dimensions with Block-Copolymer Materials: 10-Nm Sized Features with Poly(styrene)-Block-Poly(methylmethacrylate). *J. micro-nanolithography MEMS MOEMS* **2013**, *12* (3).

(44) Rasappa, S.; Borah, D.; Senthamaraikannan, R.; Faulkner, C. C.; Shaw, M. T.; Gleeson, P.; Holmes, J. D.; Morris, M. A. Block Copolymer Lithography: Feature Size Control and Extension by an over-Etch Technique. *Thin Solid Films* **2012**, *522*, 318–323.

(45) Borah, D.; Senthamaraikannan, R.; Rasappa, S.; Kosmala, B.; Holmes, J. D.; Morris, M. A. Swift Nanopattern Formation of PS-B-PMMA and PS-B-PDMS Block Copolymer Films Using a Microwave Assisted Technique. *ACS Nano* **2013**, *7* (8), 6583–6596.

(46) Busch, P.; Posselt, D.; Smilgies, D. M.; Rheinlander, B.; Kremer, F.; Papadakis, C. M. Lamellar Diblock Copolymer Thin Films Investigated by Tapping Mode Atomic Force Microscopy: A Molar-Mass Dependence of Surface Ordering. *Macromolecules* **2003**, *36* (23), 8717–8727.

(47) Metwalli, E.; Perlich, J.; Wang, W.; Diethert, A.; Roth, S. V.; Papadakis, C. M.; Müller-Buschbaum, P. Morphology of Semicrystalline Diblock Copolymer Thin Films upon Directional Solvent Vapor Flow. *Macromol. Chem. Phys.* **2010**, *211*, 2102–2108.

(48) Ferrarese Lupi, F.; Giammaria, T. J.; Ceresoli, M.; Seguini, G.; Sparnacci, K.; Antonioli, D.; Gianotti, V.; Laus, M.; Perego, M. Rapid Thermal Processing of Self-Assembling Block Copolymer Thin Films. *Nanotechnology* **2013**, *24* (31).

(49) Harrison, C.; Angelescu, D. E.; Trawick, M.; Cheng, Z.; Huse, D. a; Chaikin, P. M.; Vega, D. a; Sebastian, J. M.; Register, R. a; Adamson, D. H. Pattern Coarsening in a 2D Hexagonal System. *Europhys. Lett.* **2004**, *67* (5), 800–806.

(50) Vega, D. A.; Harrison, C. K.; Angelescu, D. E.; Trawick, M. L.; Huse, D. A.; Chaikin, P. M.; Register, R. A. Ordering Mechanisms in Two-Dimensional Sphere-Forming Block Copolymers. *Phys. Rev. E - Stat. Nonlinear, Soft Matter Phys.* **2005**, *71* (6), 1–12.

(51) Park NX20 www.parkafm.com.

(52) SuperSharp, Tapping Mode AFM Probe SSS-NCHR www.nanoandmore.com.

(53) Ferrarese Lupi, F.; Giammaria, T. J.; Seguini, G.; Laus, M.; Enrico, E.; De Leo, N.; Boarino, L.; Ober, C. K.; Perego, M. Thermally Induced Orientational Flipping of Cylindrical Phase Diblock Copolymers. *J. Mater. Chem. C* **2014**, *2* (12), 2175–2182.

(54) Ferrarese Lupi, F.; Aprile, G.; Giammaria, T. J.; Seguini, G.; Zuccheri, G.; De Leo, N.; Boarino, L.; Laus, M.; Perego, M. Thickness and Microdomain Orientation of Asymmetric PS-B-PMMA Block Copolymer Films Inside Periodic Gratings. *ACS Appl. Mater. Interfaces* **2015**, *7* (42), 23615–23622.

(55) Wilkening, G.; Koenders, L.; Garnaes, J.; Kühle, A.; Nielsen, L.; Borsetto, F. *Nanoscale Calibration Standards and Methods: Dimensional and Related Measurements in the Micro- and Nanometer Range Chapter 14: True Three-Dimensional Calibration of Closed Loop Scanning Probe Microscopes*; 2006.

(56) Korpelainen, V.; Seppä, J.; Lassila, A. Measurement Strategies and Uncertainty Estimations for Pitch and Step Height Calibrations by Metrological Atomic Force Microscope. *J. micro-nanolithography MEMS MOEMS* **2012**, *11* (1).

(57) SPIP – Scanning Probe Image Processor www.imagemet.com.

TABLE OF CONTENTS GRAPHIC